Meteorological Conditions Associated with Five Dust Events

David R. Vollmer[1], Sandra L. LeGrand[1], Theodore W. Letcher[2]

[1] U.S. Army Engineer Research and Development Center, Geospatial Research Laboratory

[2] U.S. Army Engineer Research and Development Center, Cold Regions Research and Engineering Laboratory

Introduction

Airborne dust is an essential component of climatological and biogeochemical processes. Blowing dust can also adversely affect agriculture, transportation, air quality, sensor performance, and human health. As a result, the accurate characterization and forecasting of dust events is a priority for air quality researchers and operational weather centers. While dust detection and prediction capabilities have evolved considerably over the previous decades, improvements in forecasting the specific location and timing of individual dust events, especially extreme dust outbreaks, are needed. Accordingly, Operational weather forecasters and the US Army Engineer Research and Development Center (ERDC) are collaboratively establishing a series of reference case study events to enhance dust transport model development and evaluation. These reference case studies support ongoing research to increase the accuracy of simulated dust emissions, dust aerosol transport, and dust-induced hazardous air quality conditions. This presentation documents five new case study contributions to the reference inventory, including detailed assessments of dust storms from three different regions of the Global South with differing meteorological forcing regimes.

Here, we examine :

- A multi-day Berg wind event in southern Africa
- A strong but short-lived dust plume from the Atacama Desert of Chile,
- A narrow, isolated dust plume emanating from a dry lakebed in Patagonia.
- Two extreme dust episodes that affected India

Data Sources

MSG-SEVIRI and GOES Dust-Enhanced False-Color Imagery

- 15-min frequency dust-enhanced false-color imagery from Spinning Enhanced Visible InfraRed Imager (SEVIRI) on geostationary Meteosat Second Generation (MSG) satellite[1,2]
- Gridded data US Geostationary Operational Environmental Satellite (GOES) via the National Oceanic and Atmospheric Administration (NOAA) Comprehensive Large Array-Data Stewardship System (CLASS). Channels 11, 13, 14, and 15 (8.5, 10.3, 11.2, and 12.3) from GOES-16 Advanced Baseline Imager (ABI)[3]

MODIS Imagery and Aerosol Optical Depth

- NASA Worldview portal (https://worldview.earthdata.nasa.gov)
- Moderate Resolution Imaging Spectroradiometer (MODIS) Aqua and Terra[4]
- Suomi National Polar-orbiting Program imagery
- AOD value <0.1 indicates "clean" skies (i.e., maximum visibility)
- AOD value >3.00 indicates aerosol layer is so dense that it obscures the sun

ERA5 Reanalysis Data

- ECMWF 0.25-degree Global Reanalysis[5]
- U (west-east; zonal) and V (south-north; meridional), geopotential height, RH, relative vorticity, and temperature at 150, 200, 300, 500, 700, 850 hPa
- 10-meter U and V, 2-meter temperature and dew point, and surface-based CAPE

CALIPSO

- 532 nm total attenuated backscatter and aerosol subtype profile
- Cloud-Aerosol LiDAR and Infrared Pathfinder Satellite Observation (CALIPSO) Cloud-Aerosol Lidar with Orthogonal Polarization (CALIOP) sensor[6,7]

AERONET

- Aerosol Robotic Network (AERONET) - global network of ground-based sunphotometers[8]

Lightning

- Vaisala global lightning data obtained from the US Air Force 14th Weather Squadron[9]

Background

We selected these cases both for the variety of meteorological forcing mechanisms and for the representativeness of each event relative to its theater.

- South Africa/Namibia - Berg wind is a locally well-known regime varying year to year (2 – 12 per year period 1992 – 1998, average 6 per year[10]), the resulting dust event frequency is also highly variable from year to year with 75 dust days detected by satellite 2006 – 2016[11]
- Patagonia – Lago Colhué Huapí common dust source – average 48 dust days per year (dust detected at Comodoro Rivadavia) period 1965 – 2017, peaking Dec – Mar (summer)[12]
- Atacama Desert – One of driest deserts on Earth – dust storms are heavily influenced by local topography, but few reliable weather/climatological observations currently available[13]
- Thar Desert – 5 – 10 dust storms over northern India per year, peaking May – Jun (spring) and corresponding to transition between dry and wet phase of monsoon[14,15,16]

These cases will compliment other work by this team in completing a case catalog for the world's dust producing regions for dust model testing and development.

References

1. Banks, J. R., and H. E. Brindley, 2013: Evaluation of MSG-SEVIRI mineral dust retrieval products over North Africa and the Middle East. *Remote Sensing of Environment*, **128**, 58–73, https://doi.org/10.1016/j.rse.2012.07.017.
2. Brindley, H., P. Knippertz, C. Ryder, and I. Ashpole, 2012: A critical evaluation of the ability of the Spinning Enhanced Visible and Infrared Imager (SEVIRI) thermal infrared red-green-blue rendering to identify dust events: Theoretical analysis. *Journal of Geophysical Research: Atmospheres*, **117**, https://doi.org/10.1029/2011JD017326.
3. https://rammb.cira.colostate.edu/training/visit/quick_guides/Dust_RGB_Quick_Guide.pdf [last access: 26 October 2023]
4. Levy, R. C., S. Mattoo, L. A. Munchak, L. A. Remer, A. M. Sayer, F. Patadia, and N. C. Hsu, 2013: The Collection 6 MODIS aerosol products over land and ocean. *Atmospheric Measurement Techniques*, **6**, 2989–3034, https://doi.org/10.5194/amt-6-2989-2013
5. Hersbach, H., and Coauthors, 2020. The ERA5 Global Reanalysis, *Quarterly Journal of the Royal Meteorological Society*, **146**, 1999–2049, https://doi.org/10.1002/qj.3803.
6. Liu, Z., and Coauthors, 2008: Airborne dust distributions over the Tibetan Plateau and surrounding areas derived from the first year of CALIPSO lidar observations. *Atmospheric Chemistry and Physics*, **8**, 5045–5060, https://doi.org/10.5194/acp-8-5045-2008.
7. He, Y. and F. Yi, 2015. Dust Aerosols Detected Using a Ground-Based Polarization Lidar and CALIPSO over Wuhan (30.5° N, 114.4° E), China, *Advanced Meteorology*. 2015, 536762
8. Holben, B. N., and Coauthors, 2001: An emerging ground-based aerosol climatology: Aerosol optical depth from AERONET. *Journal of Geophysical Research: Atmospheres*, **106**, 12067–12097, https://doi.org/10.1029/2001JD900014.
9. Lojou, Jean-Yves, and Kenneth Cummins. 2005. On the Representation of Two- and Three-Dimensional Total Lightning Information.
10. Tlhalerwa, K., M. T. Freiman & s. J. Piketh, 2005. Aerosol deposition off the southern African west coast by berg winds, *S South African Geographical Journal*, **87**, 152–161, https://doi.org/10.1080/03736245.2005.9713838.
11. Eckardt,F. D., S. Bekiswa, J.R. Von Holdt, C. Jack, N.J Kuhn, F. Mogane, J.E Murray, N. Ndara, A.R. Palmer, 2020. South Africa's agricultural dust sources and events from MSG SEVIRI, *Aeolian Research*, **47**, https://doi.org/10.1016/j.aeolia.2020.100637
12. Gassó, S., and O. Torres. 2019. Temporal Characterization of Dust Activity in the Central Patagonia Desert (Years 1964–2017). Journal of Geophysical Research: Atmospheres 124 (6): 3417–34. https://doi.org/10.1029/2018JD030209
13. Arenas-Díaz, Franko and coauthors, 2022. "Dust and Aerosols in the Atacama Desert." Earth-Science Reviews 226 (March): 103925. https://doi.org/10.1016/j.earscirev.2022.103925.
14. Goudie, Andrew S, and Nicholas J Middleton.2000. Dust Storms in South West Asia. *Acta Universitatis Carolinae,* 73-83
15. Banerjee, P., S. K. Satheesh, and K. K. Moorthy, 2021: The Unusual Severe Dust Storm of May 2018 Over Northern India: Genesis, Propagation, and Associated Conditions. *Journal of Geophysical Research: Atmospheres*, **126**, e2020JD032369, https://doi.org/10.1029/2020JD032369.
16. Parde, A. N., N. G. Dhangar, S. Nivdange, S. D. Ghude, P. Pithani, C. Jena, D. M. Lal, and V. Gopalakrishnan, 2022: The analysis of pre-monsoon dust storm over Delhi using ground-based observations. *Nat Hazards*, **112**, 829–844, https://doi.org/10.1007/s11069-022-05207-z.

Case 1: 16-17 July 2020 – Namibia

- Classic example of "Berg Wind" regime
- Strong surface anticyclone caused downslope winds off of Central Plateau
- Plumes present all along southwest coast for 48 hrs+
- Plumes ended when isobaric gradient relaxed as anticyclone moved east

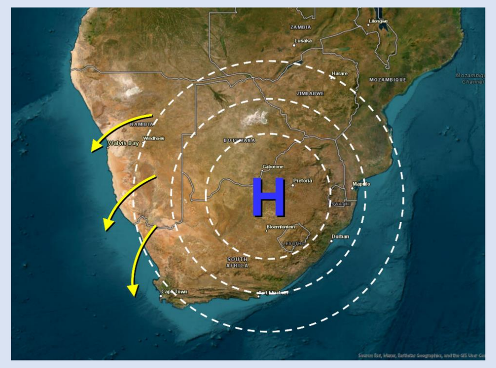

Figure 1 (above): Depiction of typical "Berg Wind" regime. White dashed lines represent idealized isobars. The yellow arrows represent the surface winds flowing out from the anticyclone. This regime is representative of the conditions associated with the 16-17 July 2020 dust event.

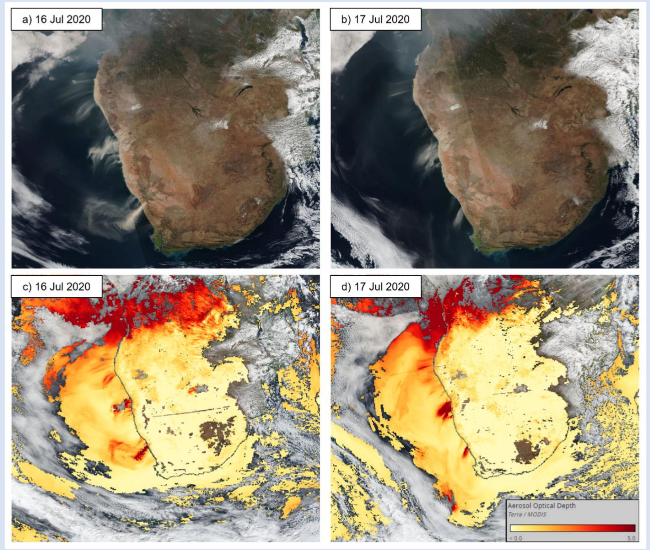

Figure 2 (above): Suomi National Polar-orbiting Partnership VIRS true-color imagery for 16 – 17 July (a and b), and same with MODIS Deep Blue Aerosol Optical Depth overlaid (c and d). The color scale for AOD is logarithmic, not linear. Note the presence of multiple dust plumes off the southwest coast of Africa.

Figure 3 (below): ERA5 reanalysis of mean sea level pressure (hPa) and 1000 – 500 hPa thickness valid at 0000 UTC 15 – 18 July 2020. purple dot represents Walvis Bay, Namibia. Of note is the strong anticyclone located over South Africa and the resulting surface pressure pattern over the Namibian coast

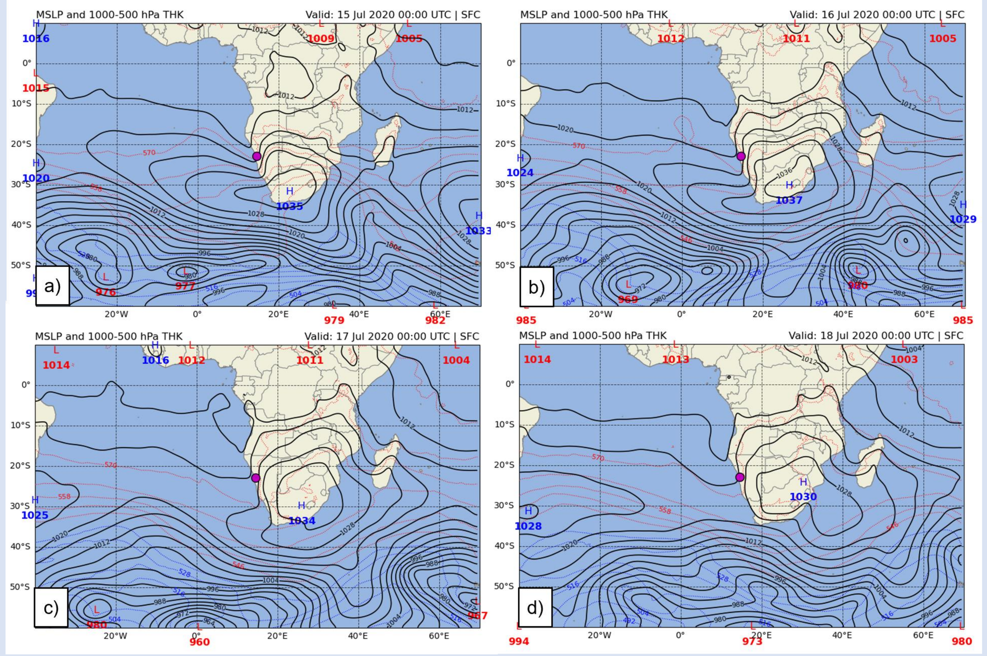

Case 2: 7 March 2020 – Patagonia

- Mid-latitude cyclogenesis over the southern tip of South America
- Strong upper-level trough, cut-off low
- Surface winds driven by tight isobaric gradient
- Solitary dust plume from dry lakebed at Lago Colhué Huapí, Argentina

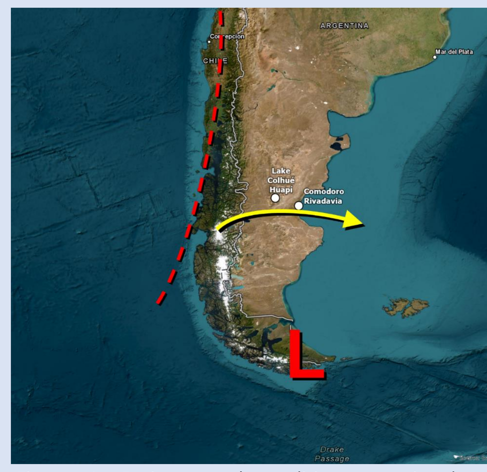

Figure 4: Environmental conditions associated with or responsible for dust emissions during the 7 March 2020 dust event at Lake Colhué Huapí. The large red 'L' represents the position of the surface low over Cape Horn while the red dashed line marks the position of the upper-level long wave trough. The yellow arrow shows the resultant surface flow..

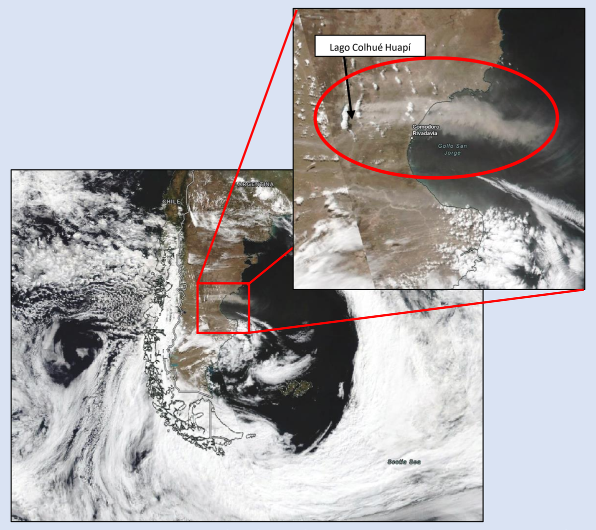

Figure 5: Suomi National Polar-orbiting Partnership VIRS true-color imagery for 7 March 2020. Overpass occurred at approximately 1749 UTC.

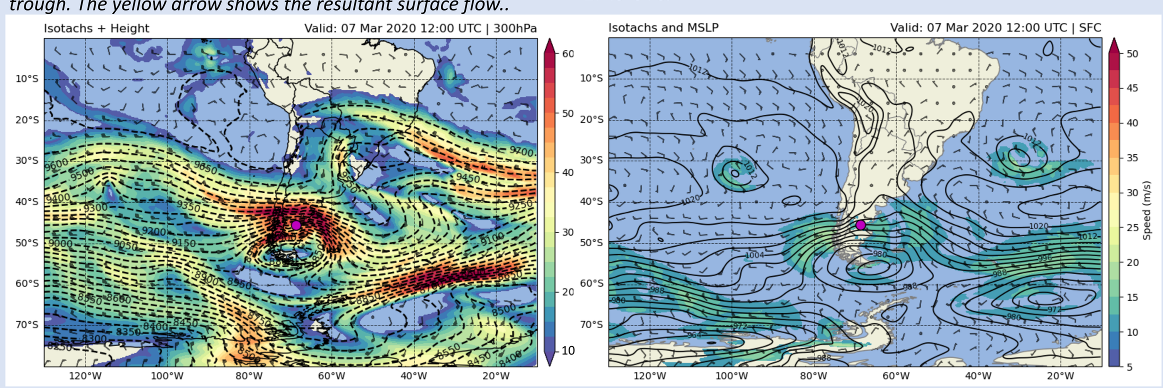

Figure 6: ERA5 300 hPa (left) geopotential height (m), isotachs, and wind barbs (ms^{-1}), and (right) MSLP (hPa), 10-m isotachs, and wind barbs (ms^{-1}), Note the positions of the upper-level cyclone and the surface cyclone. The purple dot is the lakebed source region.

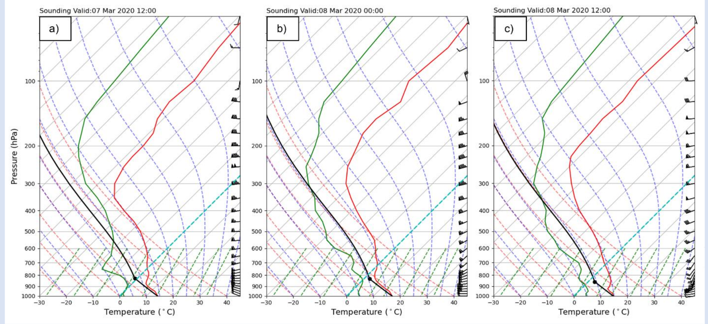

Figure 7: ERA5-dervied Skew-T, Log P soundings centered on Lake Colhué Huapí, marked by the purple dot in Figures 10-12, valid at 1200 UTC 7 March (a) and at 0000 UTC and 1200 UTC (b-c) on 8 March 2020. In panels a and b, the boundary layer was relatively deep and well-mixed, whereas in panel c, the mixed layer was much shallower and the surface wind speed had decreased.

Case 3: 25 July 2019 – Chile

- Deep longwave polar jet front trough with surface trough along northern Chilean coast
- Short-lived, narrow plume
- Source was Atacama Desert near Calama, Chile
- Local wind influenced heavily by complex terrain

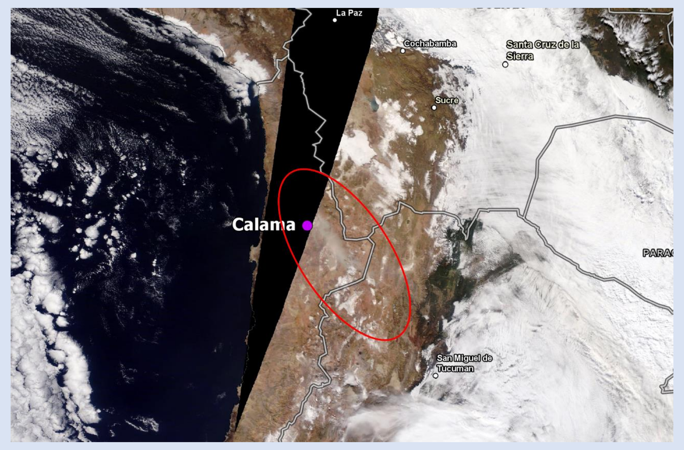

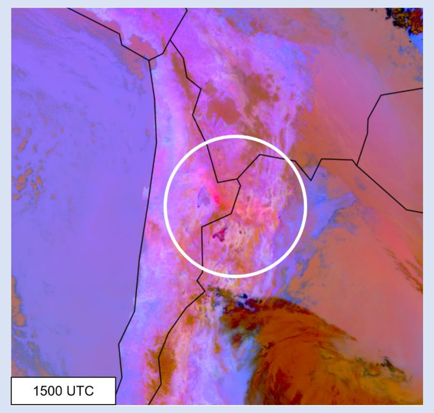

Figure 8 (above): GOES-16 false color imagery showing the dust plume (indicated by pink/fuchsia shading surrounded by white circle).

Figure 9 (upper left)):MODIS Terra true-color image from approximately 1406 UTC 25 July 2019. The dust likely originated from the area in the image mosaic gap.

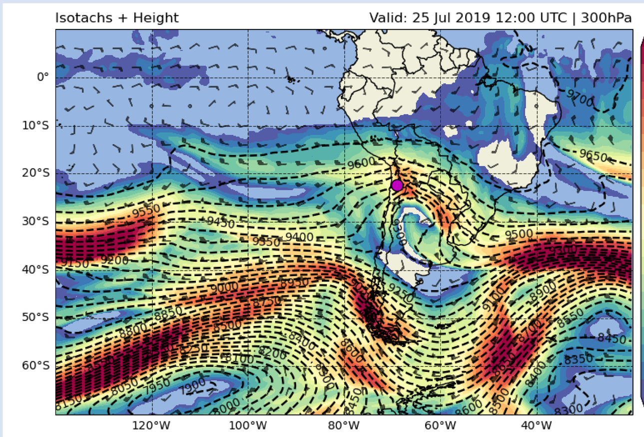

Figure 10 (left): ERA5 reanalysis of 300 hPa geopotential height (dashed, m), isotachs (shaded, ms^{-1}) and wind barbs (ms^{-1}) valid at 1200 UTC 25 July 2019. The purple dot represents Calama, the largest city near the source region for this dust storm. The axis of an upper-level trough in an equatorward branch of the polar front jet stream passed over the Atacama Desert.

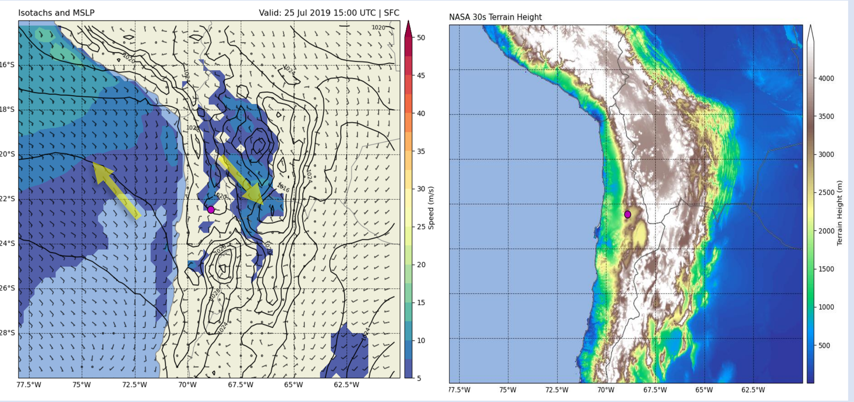

Figure 11: ERA5 reanalysis of mean sea level pressure (solid, hPa), 10 m wind speed (ms-1; shaded), and wind barbs (ms-1) (a-h) valid at 1500 UTC 25 July 2019 (left), and terrain elevation (m) (right). Note how the direction of the winds over the northern Atacama Desert differ significantly from the winds offshore (yellow arrows), and how the local wind maximum corresponds with areas of higher terrain elevation.

Case 4: 12 – 17 June 2018 – India

- Large-scale multi-day event
- Source region was the Thar Desert
- Plume began 12 June and lasted until scavenged out by convection on 17 June
- Subtropical jet developed a closed anticyclonic circulation with tropical easterly jet above source region
- Surface winds remained strong and onshore through the period due to thermal low over India/Pakistan border

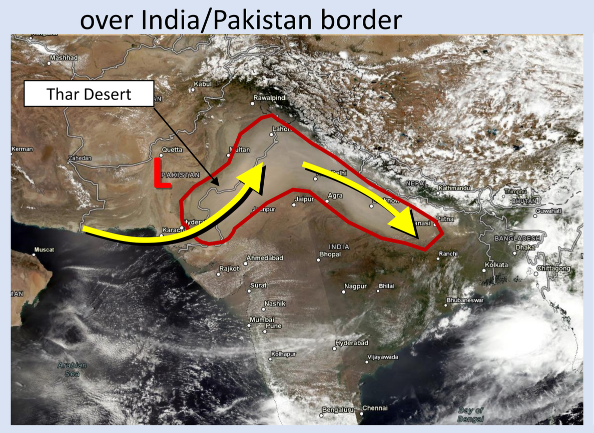

Figure 12: Environmental conditions associated with or responsible for dust emissions during the 12 – 17 June 2018 dust storm India. The red 'L' represents the position of the thermal surface low and the yellow arrow represents the direction of the surface wind. The image is from Suomi NPP on 14 June . Red outlines the dust plume.

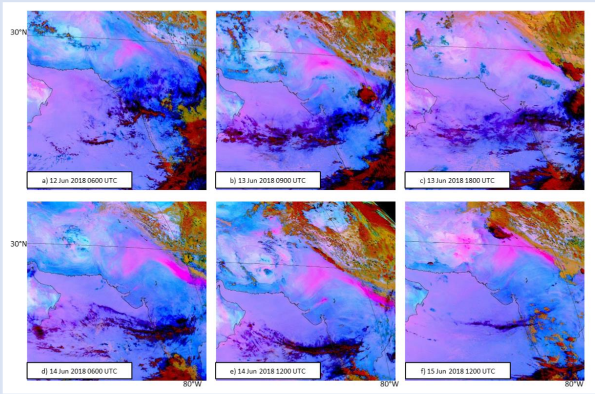

Figure 13: MSG-SEVIRI dust-enhanced imagery for selected times 13 – 15 June 2018. Concentrated areas of pink and magenta colors generally indicate airborne dust, while areas of red or brown shading are generally thick clouds. The plume was particularly concentrated and persistent

Figure 14: 150 hPa (a) and 200 hPa (b) geopotential height (m), isotachs, and wind barbs (ms^{-1}), (c) 2-meter temperatures (°C), MSLP (hPa), and wind barbs (ms^{-1}), and (d) MSLP (hPa), 10-meter isotachs, and wind barbs (ms^{-1}) from ERA5 reanalysis valid 1200 UTC, 14 June 2018. The dot represents the central Thar Desert. Note the closed anticyclonic circulation around the Thar Desert at both 150 hPa and 200 hPa and the deep thermal surface low below. Anticyclonic circulation aloft forced subsidence—trapping dust below mid-levels—and onshore flow around the thermal low supported the multi-day dust plume adverting toward the Indo-Gangetic Plain.

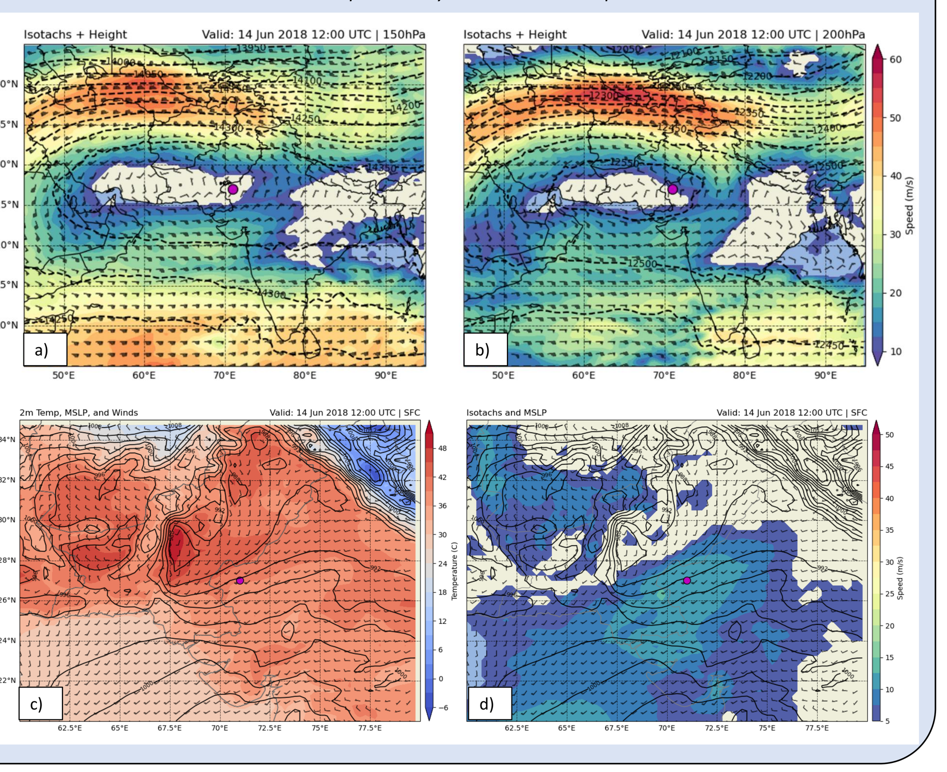

Case 5: 2 – 9 May 2018 – India

- Another large-scale multi-day event
- Source region was the Thar Desert
- Plume began 2 May and lasted through 9 May
- Initiated by widespread convection
- Thermal low over Pakistan caused prolonged onshore flow
- Over 100 deaths reported as related to the dust storm.

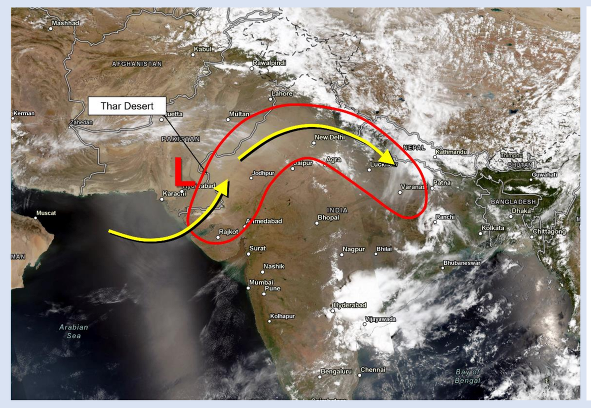

Figure 15: As in Figure 12, but for the situation from 2 – 9 May 2018. Suomi NPP mage is from 3 May 2018.

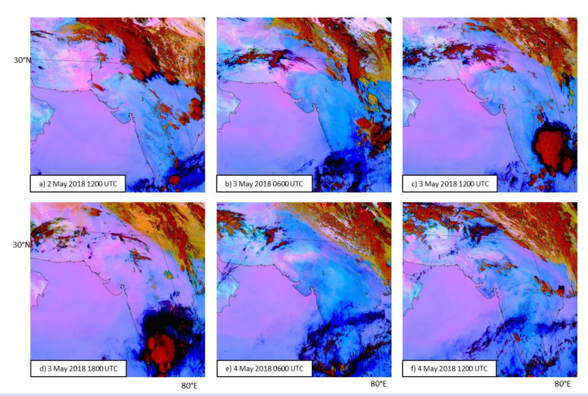

Figure 16: As in Figure 13, but for select times from 2 – 4 May 2018. Note the presence of cloud (red) in addition to dust (pink).

Figure 16: 150 hPa (a) and 200 hPa (b) geopotential height (m), isotachs, and wind barbs (ms^{-1}), (c) 2-meter temperatures (°C), MSLP (hPa), and wind barbs (ms^{-1}), and (d) MSLP (hPa), 10-meter isotachs, and wind barbs (ms^{-1}) from ERA5 reanalysis valid 1200 UTC, 3 May2018. The dot represents the central Thar Desert. Aloft, a strong anticyclonically-curved subtropical jet streak developed over Afghanistan and northern Pakistan with the Thar Desert positioned under the right exist region, where subsidence was occurring through most of the depth of the troposphere. At the surface, a thermal low was present to the southeast of the Thar Desert, with surface winds directed from the desert toward the population centers to the northeast.

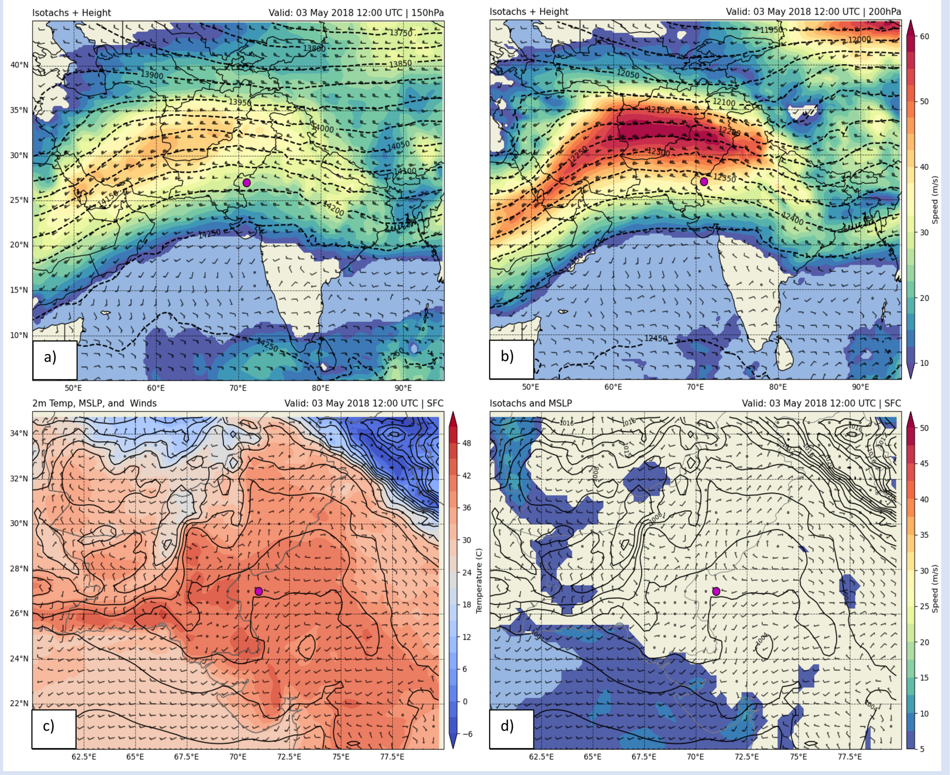

Figure 17: Vaisala lightning data for 2 May 2018, showing cloud-to-ground flash locations for the first 12 hours (a) and the second 12 hours (b) of the day. Time of each flash is color-coded. Note the widespread convective activity north and east of the Thar Desert, indicating that thunderstorm outflows may have played a role in initiating this event.

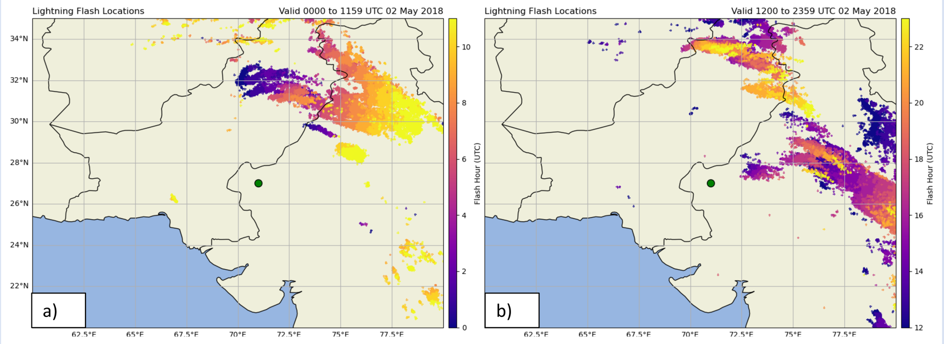

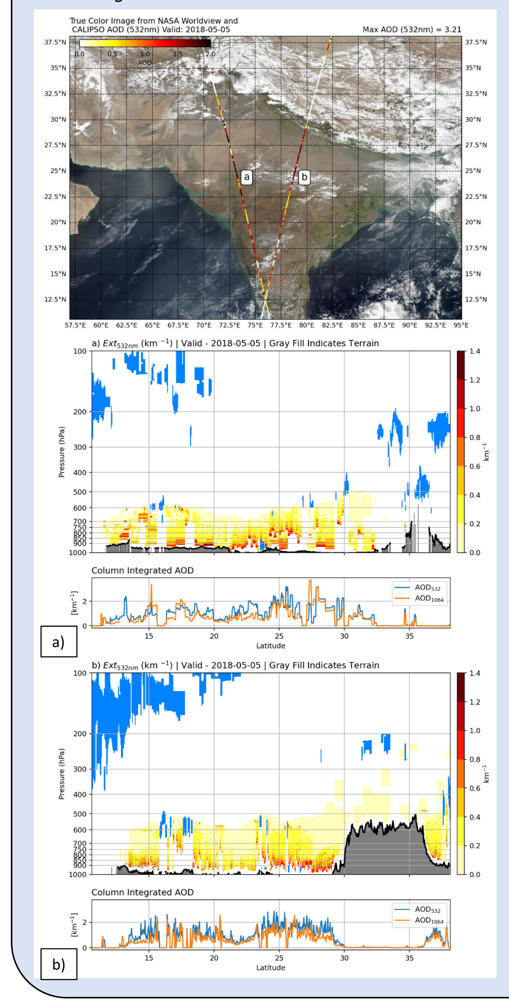

Figure 18 (left): Worldview true-color imagery (top) with the CALIPSO AOD on its ascending (labeled 'a') and descending pass (labeled 'b') and CALIPSO extinction coefficient vertical cross section 'a' and 'b' from south to north (color shaded). The solid-blue shading indicates cloud. The outlined gray surface shows the approximate ground surface. Below each cross-section is the column integrated AOD for the yellow-visible (532 nm) and NIR (1064 nm). Overpasses occurred on 5 May 2018. The yellow shading extending to 600 hPa and above is probably the dust plume. The Himalaya Mountains blocked much of the dust, trapping it across the highly populated Indo-Gangetic Plain.

Figure 19 (right): AERONET Aerosol optical depth fully quality-controlled level 2.0 data for Kanpur, India (top) and for Gandhi College in rural Uttar Pradesh, India for May 2018. Both AERONET stations show elevated AOD levels throughout the month, as several major multi-day dust storms impacted northern India in May and June of 2018. The AOD values exceeding about 1.5 suggest that aerosol species such as smoke and smog were present with the dust.

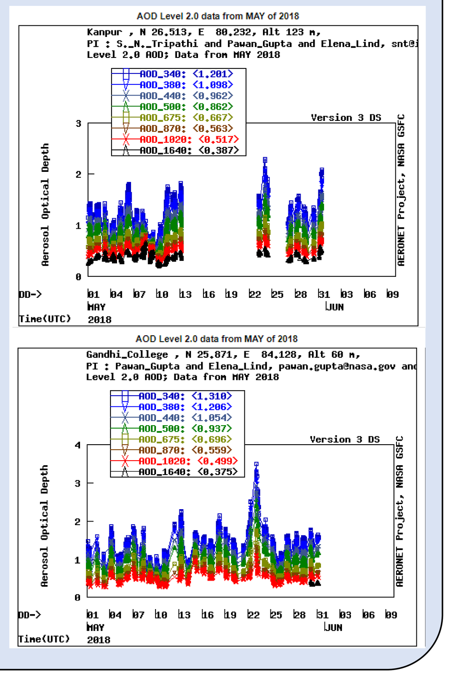

Future Work

These case studies—focused on the Global South—are added to a global inventory of cases with a broad spectrum of meteorological forcing and diverse geography with which existing and new model dust transport schemes may be tested. Future work involves improving current operational model configurations as well as developing new dust simulation technologies for the next generation of operational models.